HEAT TRANSFER AND SKIN FRICTION ANALYSIS IN GOERTLER FLOW

Vinicius Malatesta, malatest@icmc.usp.br
Leandro Franco de Souza, lefraso@icmc.usp.br
Departamento de Matemática Aplicada e Estatística–ICMC–USP
CEP – 13560-970 – São Carlos – SP – Brazil

Abstract. *The increase in heat transfer rates aiming efficient systems is one of the goals in convection heat transfer exchangers. The centrifugal hydrodynamic instability that occurs in boundary layers over concave walls can be used to increase the heat transfer rate. This instability gives rise to streamwise vortices known as Goertler Vortices (GV). These vortices causes also an increase in the skin friction. In the present work the increase in heat transfer rate and in the skin friction are analyzed. The work is carried out by a Spatial Direct Numerical Simulation. The Navier-Stokes equation is written in vorticity-velocity formulation. The time integration is done via a classical 4^{th} order method. The spatial derivatives are calculated using high-order compact finite difference methods (streamwise and wall-normal directions) and spectral methods (spanwise direction). The flow is disturbed by steady suction and blowing flow at wall. 4 different wavelengths were disturbed in all numerical tests. The results shows that the increase in heat transfer can be greater than the increase in the skin friction when Prandtl number is greater than 1.*

Keywords: *Goertler flow, heat transfer, laminar-turbulent transition, Direct Numerical Simulation, high order methods*

1. INTRODUCTION

The practical interest in intensifying surface heat transfer rates with the least penalty follows the need to reduce energy consumption via more efficient systems. Vortices and heat transfer have been under study, with leading examples discussed by Fiebig (1996).

Vortices have always to be considered together with their generation when flow losses are of importance because their generation causes the major contribution to the flow losses. The heat transfer due to vortices, in contrast, is independent of their generation. For steady flow, longitudinal vortices are more effective than transverse vortices for heat transfer enhancement because longitudinal vortices provide an additional mode of thermal energy transport, spiraling transport, while transverse vortices generate no additional mode of streamwise energy transport. Transverse vortices lead to self sustained oscillations and transition to turbulence at lower Reynolds number than longitudinal vortices.

Recent measurements (L. Momayez and Peershossaini, 2004) conducted under well-controlled conditions were carried out on a concave heated wall in order to understand the effects of Goertler instability and its transition to turbulence on heat transfer from the wall to the boundary layer. Another aim of the experiment was to obtain reliable data and pertinent dimensionless parameters to scale the heat-transfer problem most appropriately. Analysis of the effects of the Goertler vortex wavelength and of perturbation wire diameter shows that the smaller the vortex wavelength, the faster the apparent transition to turbulence. Moreover, larger wire diameters also cause a faster boundary-layer transition. The coefficient of local convective heat transfer between the fluid and wall can be reduced to either the local Nusselt or Stanton number. At the wall heat is identified by Stanton number St, which is calculated from the measured wall temperatures and wall heat flux. According to them, the Staton number St is more appropriate in describing heat transfer in the laminar regime because its evolution allows immediate comprehension of the flow state in various longitudinal positions. Moreover, St has the advantage of being analogous to the friction coefficient, it is physically more interesting than Nusselt number.

In Girgis and Liu (2006), the spanwise averaged streamwise-velocity gradient, obtained by Goertler flow, is studied in terms of skin friction. In the absence of wavy disturbance to the steady flow, the skin friction due to nonlinear steady longitudinal Goertler vortex can already nearly bridge the transition from the local laminar skin friction values to that turbulent skin friction. Their results were based in the experimental measurements by Swearingen and Blackwelder (1987). The emphasis is placed on the nonlinear modification of the steady problem by Reynolds stresses of the wavy disturbance, when it is found that skin friction increases well above the local turbulent boundary layer value.

In the present work, by means of Spatial Direct Numerical Simulation, the heat transfer over a concave surface is analyzed. The flow over concave surface can be hydrodynamically unstable giving rise to streamwise vortices (Goertler Vortices), which increase the skin friction and heat transfer rates. The work is divided as follows: the next section shows the formulation adopted; in section 3 the numerical methods are described; the results are shown in section 4 and the last section gives the main conclusions of the work.

2. FORMULATION

In this section the governing equations and the numerical methodology implemented are presented. The Navier-Stokes equations written in the vorticity-velocity formulation were discretized using high-order finite-differences and spectral approximations for the spatial derivatives. A fourth order Runge-Kutta scheme for the temporal discretization.

2.1 Governing Equations

The governing equations are the incompressible, Navier-Stokes equations with constant viscosity. Defining the vorticity as the negative curl of the velocity vector, and using the fact that both the velocity and the vorticity fields are solenoidal, one can obtain the following vorticity transport equation in each direction:

$$\frac{\partial\widetilde{\omega}_x}{\partial t}+\frac{\partial\widetilde{a}}{\partial y}-\frac{\partial\widetilde{b}}{\partial z}+\frac{Go^2}{\sqrt{Re}h}\frac{\partial\widetilde{d}}{\partial z}=\frac{1}{Re}\nabla^2\widetilde{\omega}_x, \tag{1}$$

$$\frac{\partial\widetilde{\omega}_y}{\partial t}+\frac{\partial\widetilde{c}}{\partial z}-\frac{\partial\widetilde{a}}{\partial x}=\frac{1}{Re}\nabla^2\widetilde{\omega}_y, \tag{2}$$

$$\frac{\partial\widetilde{\omega}_z}{\partial t}+\frac{\partial\widetilde{b}}{\partial x}-\frac{\partial\widetilde{c}}{\partial y}-\frac{Go^2}{\sqrt{Re}h}\frac{\partial\widetilde{d}}{\partial x}=\frac{1}{Re}\nabla^2\widetilde{\omega}_z, \tag{3}$$

where

$$\widetilde{a} = \widetilde{\omega}_x\widetilde{v}-\widetilde{\omega}_y\widetilde{u}, \tag{4}$$

$$\widetilde{b} = \widetilde{\omega}_z\widetilde{u}-\widetilde{\omega}_x\widetilde{w}, \tag{5}$$

$$\widetilde{c} = \widetilde{\omega}_y\widetilde{w}-\widetilde{\omega}_z\widetilde{v}, \tag{6}$$

$$\widetilde{d} = \widetilde{u}^2, \tag{7}$$

are the nonlinear terms resulting from convection, vortex stretching and vortex bending. The variables $(\widetilde{u},\widetilde{v},\widetilde{w},\widetilde{\omega}_x,\widetilde{\omega}_y,\widetilde{\omega}_z)$ are the velocity and vorticity components in the streamwise, wall-normal and spanwise directions respectively; $\widetilde{t}$ is the time. The Laplace operator is:

$$\nabla^2=\left(\frac{\partial^2}{\partial x^2}+\frac{\partial^2}{\partial y^2}+\frac{\partial^2}{\partial z^2}\right). \tag{8}$$

The continuity equation is given by:

$$\frac{\partial\widetilde{u}}{\partial x}+\frac{\partial\widetilde{v}}{\partial y}+\frac{\partial\widetilde{w}}{\partial z}=0. \tag{9}$$

The heat transfer transport equation adopted in the present work is:

$$\frac{\partial\widetilde{\theta}}{\partial t}+\frac{\partial\widetilde{u}\widetilde{\theta}}{\partial x}+\frac{\partial\widetilde{v}\widetilde{\theta}}{\partial y}+\frac{\partial\widetilde{w}\widetilde{\theta}}{\partial z}=\frac{1}{Re\,Pr}\nabla^2\widetilde{\theta}, \tag{10}$$

where $\widetilde{\theta}$ is the non dimensional temperature given by $\widetilde{\theta}=(T-T_0)/(T_\infty-T_0)$, where T is the dimensional temperature, and T_∞ and T_0 are the temperature values outside from the thermal boundary layer and at the wall, respectively.

The above equations are presented in a non-dimensional form. The reference length is a plate characteristic length $\overline{L}$ and the reference velocity is the free stream velocity $\overline{U}_\infty$. The Reynolds number is given by $Re=\overline{U}_\infty\overline{L}/\overline{\nu}$, where $\overline{\nu}$ is the kinematic viscosity. The Prandtl number is given by $Pr=\nu/\alpha$, where ν is the kinematic viscosity and α is the thermal diffusivity of the fluid. The Goertler number is given by $Go=(k_c\sqrt{Re})^{1/2}$. The terms $Go^2\frac{\partial\widetilde{d}}{\partial x}/(\sqrt{Re}h)$ and $Go^2\frac{\partial\widetilde{d}}{\partial z}/(\sqrt{Re}h)$ are the leading order curvature terms, where $h=1-k_cy$, $k_c=\overline{L}/\overline{R}$ is the wall curvature and $\overline{R}$ is the curvature radius. Although the objective of the current study is on the steady flow, the simulations were performed with the introduction of steady disturbances that generate the GV. This explains the time derivative in the equations, and to get the results it takes some computational time until the time derivatives vanishes.

Taking the definition of the vorticity and the mass conservation equation, one can obtain Poisson-type equations for each velocity component:

$$\frac{\partial^2\widetilde{u}}{\partial x^2}+\frac{\partial^2\widetilde{u}}{\partial z^2}=-\frac{\partial\widetilde{\omega}_y}{\partial z}-\frac{\partial^2\widetilde{v}}{\partial x\partial y}, \tag{11}$$

$$\frac{\partial^2\widetilde{v}}{\partial x^2}+\frac{\partial^2\widetilde{v}}{\partial y^2}+\frac{\partial^2\widetilde{v}}{\partial z^2}=-\frac{\partial\widetilde{\omega}_z}{\partial x}+\frac{\partial\widetilde{\omega}_x}{\partial z}, \tag{12}$$

$$\frac{\partial^2\widetilde{w}}{\partial x^2}+\frac{\partial^2\widetilde{w}}{\partial z^2}=\frac{\partial\widetilde{\omega}_y}{\partial x}-\frac{\partial^2\widetilde{v}}{\partial y\partial z}. \tag{13}$$

2.2 Disturbance Formulation

A disturbance formulation was adopted in the current study, therefore the flow variables were decomposed in a base flow and a perturbation:

$$\widetilde{f}=f_b+f. \tag{14}$$

With such formulation, the stability analysis of any base flow (Blasius, Falkner-Skan, etc.), can be easily performed as the linear and nonlinear terms can be isolated. Some disadvantages of this formulation are the indirect access to the flow variables and a higher memory usage due to the larger number of variables.

The variables $\widetilde{f}=\{\widetilde{u},\widetilde{v},\widetilde{w},\widetilde{\omega}_x,\widetilde{\omega}_y,\widetilde{\omega}_z,\widetilde{\Theta}\}$ are the total flow variables. The base flow is considered two-dimensional, therefore only u_b, v_b, ω_{z_b} and θ_b are taken into account, where the index b indicates the base flow.

Introducing Eq. (14) in the equations (1) – (3), (10) and (11) – (13) and subtracting the base quantities, the equations for the perturbations result in:

$$\frac{\partial\omega_x}{\partial t}+\frac{\partial a}{\partial y}-\frac{\partial b}{\partial z}+\frac{Go^2}{\sqrt{Re}h}\frac{\partial d}{\partial z} = \frac{1}{Re}\nabla^2\omega_x, \tag{15}$$

$$\frac{\partial\omega_y}{\partial t}+\frac{\partial c}{\partial z}-\frac{\partial a}{\partial x} = \frac{1}{Re}\nabla^2\omega_y, \tag{16}$$

$$\frac{\partial\omega_z}{\partial t}+\frac{\partial b}{\partial x}-\frac{\partial c}{\partial y}-\frac{Go^2}{\sqrt{Re}h}\frac{\partial d}{\partial x} = \frac{1}{Re}\nabla^2\omega_z, \tag{17}$$

$$\frac{\partial^2 u}{\partial x^2}+\frac{\partial^2 u}{\partial z^2} = -\frac{\partial\omega_y}{\partial z}-\frac{\partial^2 v}{\partial x\partial y}, \tag{18}$$

$$\frac{\partial^2 v}{\partial x^2}+\frac{\partial^2 v}{\partial y^2}+\frac{\partial^2 v}{\partial z^2} = -\frac{\partial\omega_z}{\partial x}+\frac{\partial\omega_x}{\partial z}, \tag{19}$$

$$\frac{\partial^2 w}{\partial x^2}+\frac{\partial^2 w}{\partial z^2} = \frac{\partial\omega_y}{\partial x}-\frac{\partial^2 v}{\partial y\partial z}, \tag{20}$$

$$\frac{\partial\theta}{\partial t}+\frac{\partial e}{\partial x}+\frac{\partial f}{\partial y}+\frac{\partial g}{\partial z} = \frac{1}{Re\,Pr}\nabla^2\theta, \tag{21}$$

where the nonlinear terms a, b, c, d, e and g are:

$$a = \omega_x(v_b+v)-\omega_y(u_b+u), \tag{22}$$

$$b = (\omega_{z_b}+\omega_z)(u_b+u)-\omega_x w, \tag{23}$$

$$c = \omega_y w-(\omega_{z_b}+\omega_z)(v_b+v), \tag{24}$$

$$d = 2u_b u+u^2. \tag{25}$$

$$e = u_b*\theta+u*\theta_b+u*\theta, \tag{26}$$

$$f = v_b*\theta+v*\theta_b+v*\theta, \tag{27}$$

$$g = w(\theta_b+\theta). \tag{28}$$

3. NUMERICAL METHOD

In this section the discretization of the adopted equations and the boundary conditions adopted in the simulations are shown.

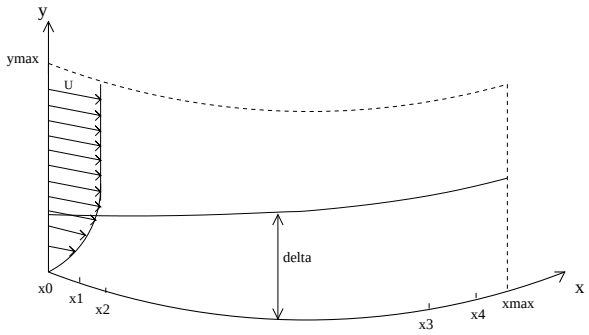

Figure 1. Solution domain.

3.1 Discretization of Field Equations

The flow is assumed to be periodic in the spanwise direction. Therefore, the flow field can be expanded in Fourier series with K spanwise Fourier modes:

$$f(x,y,z,t) = \sum_{k=0}^{K} F_k(x,y,t)e^{(i\beta_k z)}. \tag{29}$$

where $f = u, v, w, \omega_x, \omega_y, \omega_z, \theta, a, b, c, d, e, f, g$; $F_k = U_k, V_k, W_k, \Omega_{x_k}, \Omega_{y_k}, \Omega_{z_k}, \Theta_{z_k}, A_k, B_k, C_k, D_k, E_k, F_k, G_k$; and β_k is the spanwise wavenumber given by $\beta_k = 2\pi k/\lambda_z$, and λ_z is the spanwise wavelength of the fundamental spanwise Fourier mode, and $i = \sqrt{-1}$.

Substituting the Fourier transforms (Eq. 29) in the vorticity transport equations (15 – 17), in the velocity Poisson equations (18 – 20), and in the heat transfer transport equation (21) yield the governing equations in the Fourier space:

$$\frac{\partial \Omega_{x_k}}{\partial t} + \frac{\partial A_k}{\partial y} - \beta_k B_k - \frac{Go^2}{\sqrt{Re}}\frac{\beta_k (D_k^2)}{h} = \frac{1}{Re}\nabla_k^2 \Omega_{x_k}, \tag{30}$$

$$\frac{\partial \Omega_{y_k}}{\partial t} + \beta_k C_k - \frac{\partial A_k}{\partial x} = \frac{1}{Re}\nabla_k^2 \Omega_{y_k}, \tag{31}$$

$$\frac{\partial \Omega_{z_k}}{\partial t} + \frac{\partial B_k}{\partial x} + \frac{\partial C_k}{\partial y} - \frac{Go^2}{\sqrt{Re}h}\frac{\partial (D_k^2)}{\partial x} = \frac{1}{Re}\nabla_k^2 \Omega_{z_k}, \tag{32}$$

$$\frac{\partial^2 U_k}{\partial x^2} - \beta_k^2 U_k = -\beta_k \Omega_{y_k} - \frac{\partial^2 V_k}{\partial x \partial y}, \tag{33}$$

$$\frac{\partial^2 V_k}{\partial x^2} + \frac{\partial^2 V_k}{\partial y^2} - \beta_k^2 V_k = -\frac{\partial \Omega_{z_k}}{\partial x} + \beta_k \Omega_{x_k}, \tag{34}$$

$$\frac{\partial^2 W_k}{\partial x^2} - \beta_k^2 W_k = \frac{\partial \Omega_{y_k}}{\partial x} + \beta_k \frac{\partial V_k}{\partial y}, \tag{35}$$

$$\frac{\partial \Theta_k}{\partial t} + \frac{\partial E_k}{\partial x} + \frac{\partial F_k}{\partial y} - i\beta_k G = \frac{1}{Re\ Pr}\nabla_k^2 \Theta_k, \tag{36}$$

where $\nabla_k^2 = \left(\frac{\partial^2}{\partial x^2} + \frac{\partial^2}{\partial y^2} - \beta_k^2\right)$.

The equations (30 – 36) were solved numerically in the domain shown schematically in Fig. 1. The calculations are done on an orthogonal uniform grid, parallel to the wall. The fluid enters the computational domain at $x = x_0$ and exits at the outflow boundary $x = x_{max}$. Disturbances were introduced into the flow field using spanwise suction and blowing in a disturbance strip at the wall. This strip is located between x_1 and x_2. In the region located between x_3 and x_4 a buffer domain technique Kloker *et al.* (1993) was implemented in order to avoid wave reflections at the outflow boundary. In these simulations a 2D Navier-Stokes solution, taking into account the curvature term, was used as the base flow, and for the thermal boundary layer, the standard similarity solution obtained using the Pohlhausen formula was used.

The time derivatives in the vorticity transport equations were discretized with a classical 4^{th} order Runge-Kutta integration scheme Ferziger and Peric (1997). The spatial derivatives were calculated using a 6^{th} order compact finite difference-scheme L. F. Souza and Medeiros (2005); Souza (2003); Lele (1992). The V-Poisson equation – Eq. (34) –

was solved using a multigrid Full Approximation Scheme (FAS) Stüben and Trottenberg (1981). A V-cycle working with 4 grids was implemented.

3.2 Boundary Conditions

The governing equations are complemented by the specification of boundary conditions. At the wall ($y = 0$), a no-slip condition was imposed for the streamwise (U_k) and the spanwise (W_k) velocity components. The wall-normal velocity component at the wall (V_k) was specified at the suction and blowing strip region between x_1 and x_2, where the disturbances were introduced. Away from the disturbance generator this velocity component was set to zero. The function used for the wall-normal velocity $V_{k=1-4}$ at the disturbance generator is:

$$\begin{aligned} V_{k=1-4}(i,0,t) &= A\sin^3(\epsilon) \quad \text{for} \quad l_1 \leq i \leq l_2 \quad \text{and} \\ V_{k=1-4}(x,0,t) &= 0 \quad \text{for} \quad l < l_1 \quad \text{and} \quad l > l_2, \end{aligned} \tag{37}$$

where $\epsilon = \pi(l - l_1)/(l_2 - l_1)$ and A is a real constant chosen to adjust the amplitude of the disturbance. The variable l indicates the grid point location x_l in the streamwise direction, and points l_1 and l_2 correspond to x_1 and x_2 respectively. For all modes $k > 4$ the value of $V_k = 0$ at the wall were settled.

At the inflow boundary ($x = x_0$), the velocity and vorticity components and the temperature are specified based on the similarity solutions. At the outflow boundary ($x = x_{max}$), the second derivatives with respect to the streamwise direction of the velocity and vorticity components are set to zero. At the upper boundary ($y = y_{max}$) the flow is considered non rotational. This is satisfied by setting all vorticity components and their derivatives to zero. The wall-normal velocity component at the upper boundary was settled according to the condition:

$$\frac{\partial V_k}{\partial y}|_{x,y_{max},t} = 0. \tag{38}$$

In addition, at the wall, the condition $\partial V_k/\partial y = 0$ was imposed in the solution of the U_k velocity Poisson equation (Eq. 33), to ensure mass conservation. The equations used for evaluating the vorticity components at the wall are:

$$\frac{\partial^2 \Omega_{x_k}}{\partial x^2} - \beta_k^2 \Omega_{x_k} = -\frac{\partial^2 \Omega_{y_k}}{\partial x \partial y} - \beta_k \nabla_k^2 V_k \tag{39}$$

$$\frac{\partial \Omega_{z_k}}{\partial x} = \beta_k \Omega_{x_k} - \nabla_k^2 V_k. \tag{40}$$

A damping zone near the outflow boundary was defined in which all the disturbances are gradually damped down to zero (Kloker *et al.*, 1993). This technique is used to avoid reflections in the outflow boundary. Meitz and Fasel (2000) adopted a fifth order polynomial, and the same function was used in the present model. The basic idea is to multiply the vorticity components by a ramp function $f_1(x)$ after each sub-step of the integration method. Using this technique, the vorticity components are taken as:

$$\Omega_k(x,y,t) = f_1(x)\Omega_k^*(x,y,t), \tag{41}$$

where $\Omega_k^*(x,y,t)$ is the disturbance vorticity component that results from the Runge-Kutta integration and $f_1(x)$ is a ramp function that goes smoothly from 1 to 0. The implemented function was:

$$f_1(x) = f(\epsilon) = 1 - 6\epsilon^5 + 15\epsilon^4 - 10\epsilon^3, \tag{42}$$

where $\epsilon = (l - l_3)/(l_4 - l_3)$ for $l_3 \leq l \leq l_4$. The points l_3 and l_4 correspond to the positions x_3 and x_4 in the streamwise direction, respectively. To ensure good numerical results and efficiency a minimum distance between x_3 and x_4 and between x_4 and the end of the domain x_{max} had to be studied. In the simulations presented here the zones had 30 grid points in each region.

Another buffer domain, located near the inflow boundary was also implemented in the code. As pointed out by Meitz (1996), in simulations involving streamwise vortices, reflections due to the vortices at the inflow can contaminate the numerical solution. The damping function is similar to the one used for the outflow boundary:

$$f_2(x) = f(\epsilon) = 6\epsilon^5 - 15\epsilon^4 + 10\epsilon^3, \tag{43}$$

where ϵ is $\epsilon = (l - 1)/(l_1 - 1)$ for the range $1 \leq l \leq l_1$. All the vorticity components were multiplied by this function in this region.

The boundary conditions for the temperature were:

- inflow – $\theta = 0$;

- outflow – $\theta = 0$, since the same buffer domain for the vorticity was also applied for the temperature;
- wall – $\theta = 0$;
- upper boundary – the values were obtained from the heat transfer transport equation.

4. RESULTS

The parameters adopted in the simulations were: the Reynolds Number was $Re = 33124$; the Goertler Number was $Go = 2.385$; the distance between two consecutive points in the x and y directions were $dx = 0.015$ for all Prandtl number, and $dy = 0.00069$ for $Pr = 0.72$ and $Pr = 1.00$, and $dy = 0.00055$ for $Pr = 7.07$; the number of points in the x and y directions were 857, and 561 for $Pr = 0.72$ and $Pr = 1.0$, and 449 for $Pr = 7.07$, respectively with $x_0 = 1.0$ and $L = 100mm$; the delta in time was $dt = 0.003$; the disturbances were introduced in the position $1.735 \leq x \leq 2.185$, with an amplitude of $A_{k=1-4} = 1.0 \times 10^{-3}$; in the z direction, 21 Fourier modes were used with 64 points in the physical space. The disturbances were introduced for four different wavelengths: $\lambda = 4.5mm$, $\lambda = 9mm$, $\lambda = 18mm$ and $\lambda = 36mm$ and three different values of Prandtl Number were also simulated for each wavelength: $Pr = 0.72$, $Pr = 1$ and $Pr = 7.07$. The values $Pr = 0.72$ and $Pr = 7.07$ are typical for gaseous and liquid media, respectively.

The first result shows an analysis of the hydrodynamic boundary layer and the evolution of hydrodynamic instability for $Pr = 1$, where the hydrodynamic boundary layer is equal to the thermal boundary layer, then will analyze the Skin Friction and finally the analysis for each number Prandtl ($Pr = 1, 0.72$ e 7.07); where all analysis are performed introducing steady disturbances for the wavelengths $\lambda = 4.5mm$, $\lambda = 9mm$, $\lambda = 18mm$ and $\lambda = 36mm$ simultaneously.

4.1 Evolution of hydrodynamic instability

First, the base flow is analyzed when the steady disturbances were introduced by four modes $(0, k)$, $k = 1 - 4$. These disturbances are introduced by imposing a steady wall-normal velocity distribution within the disturbance strip at the wall.

For the calculation of a nonlinear, saturated Goertler-vortex scenario the Goertler vortex-mode packet is introduced with an amplitude $A_{k=1-4} = 1.0 \times 10^{-3}$. The Fourier analysis shows that the disturbance components are strongly amplified first by primary instability and saturate with different amplitudes. Figure 2 shows that the mode $(0, 4)$ attains the highest amplitude and clearly dominates the saturation region, although the amplitude of modes $(0, 1)$ and $(0, 2)$ reach high values in this region.

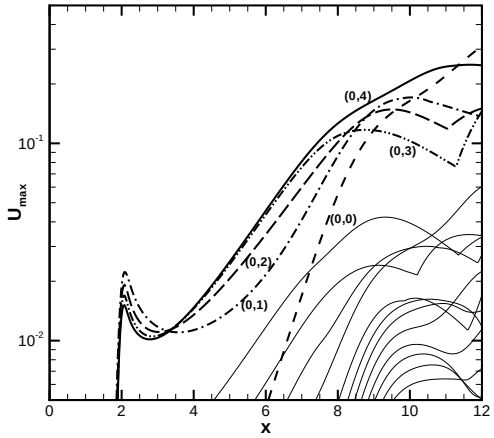

Figure 2. Amplitude of maximum u velocity component in the streamwise direction. Steady modes from $(0, 1)$ to $(0, 16)$. The mean flow distortion is also shown $(0, 0)$.

The hydrodynamic boundary layer and thermal boundary layer have the same isocontours when $Pr = 1$. Figure 3 shows the spatial evolution of the hydrodynamic (or thermal) boundary layer. These figures shown the isovelocity lines, from $u = 0.1$ to $u = 0.9$ in crosscut planes $z \times y$. The streamwise positions goes from $x = 8, 0$ to $x = 11$ in space of 1.

Two regions can be seen in a flow with Goertler vortices, the upwash and downwash regions. In the downwash region the vortices pump high velocity flow to a region close to the wall, smashing the boundary layer. In the upwash region the opposite occurs. In the non-linear region, the downwash region is stronger than the upwash region, causing an increase in the skin friction. The skin friction in a boundary layer can be calculated given by:

$$c_f = 2\nu \frac{\frac{\partial u}{\partial y}|_{wall}}{U_\infty^2}, \tag{44}$$

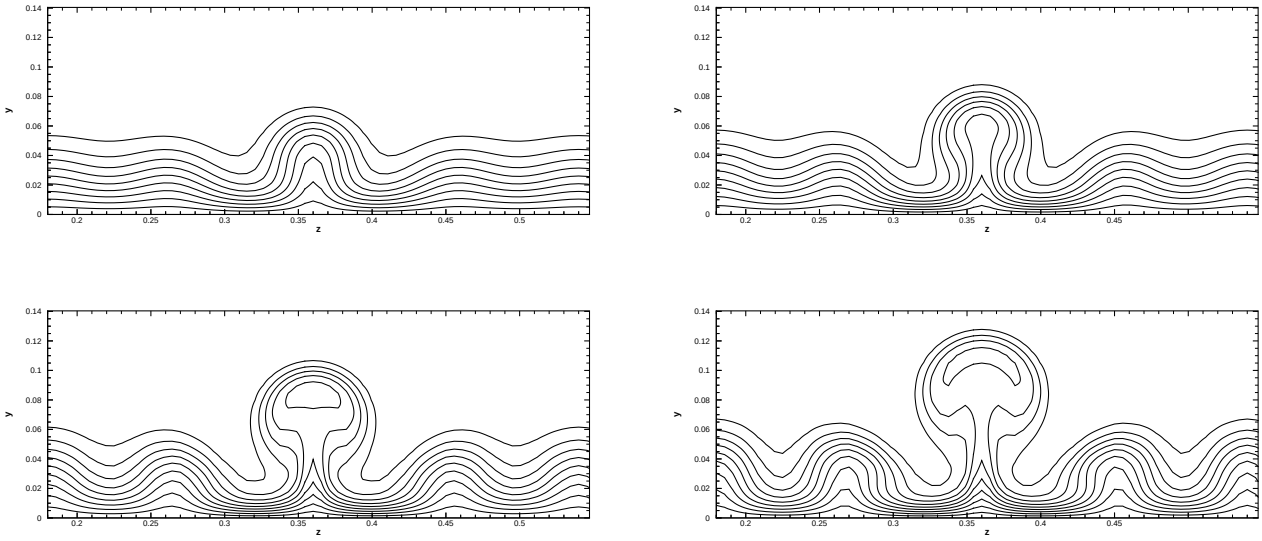

Figure 3. Isovelocity contours from $u = 0.1$ to $u = 0.9$ in a $z \times y$ planes. Top left x = 8.0, top right x = 9.0, bottom left x = 10.0 and bottom right x = 11.0.

The term that changes in the streamwise direction in this equation is the $\frac{\partial u}{\partial y}|_{wall}$. Figure 4 shows the value obtained without the presence of the vortices is shown for comparison (dashed line), and also the average value in the spanwise direction is shown (thicker line). The vortices increases the value of C_f by 193% if compared with the value obtained without vortices. In $x = 12$, the values of skin friction for Blasius and Goertler are respectively $C_f = 0.00109581$ and $C_f = 0.00320666$.

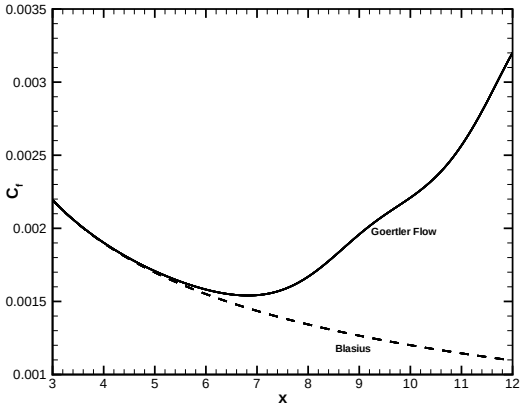

Figure 4. Streamwise evolution of the Skin friction coefficient C_f. Dashed – Value obtained for the flow without GV. Thicker line – mean value with GV.

4.2 Analysis of heat transfer for $Pr = 1$

The heat transfer analysis is carried out by checking the streamwise evolution of the Stanton number with and without Goertler vortices. The Stanton number is given by:

$$St_x = \frac{Nu_x}{PrRe_x}, \tag{45}$$

where Nu_x is the Nusselt number:

$$Nu_x = q_{wall}\frac{L}{k(T_e - T_w)}, \tag{46}$$

where q_{wall} is the heat flux at the wall:

$$q_{wall} = -k\frac{\partial T}{\partial y}|_{wall} \tag{47}$$

For $Pr = 1$ the increase in the Stanton number with and without GV reach the same rate as the skin friction, as expected. The values of Stanton for Blasius and Goertler are respectively $St = 0.00073386$ and $St = 0.00214749$, an increase in 193%.

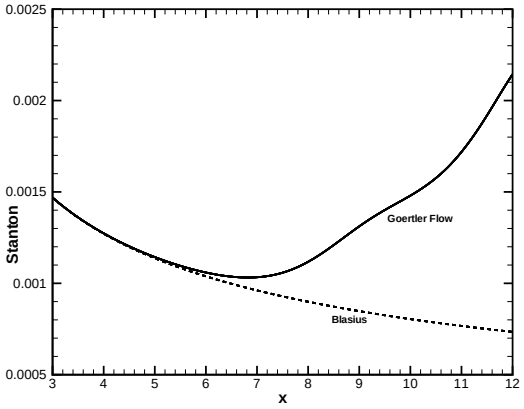

Figure 5. Streamwise evolution of the Stanton number. Dashed – Value obtained for the flow without GV. Thicker line – mean value with GV.

4.3 Analysis of heat transfer for $Pr = 0.72$

In the present case, the hydrodynamic boundary layer is smaller than the thermal boundary layer. The isovelocity and isothermal contours are shown in Fig. 6 in the streamwise position $x = 11.0$. it can be observed that the thermal boundary layer is also smashed in the wall direction, increasing the Stanton number.

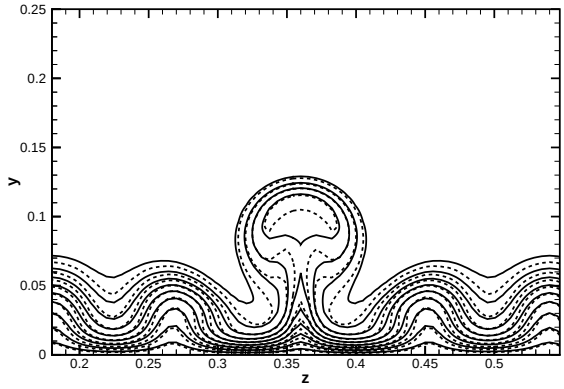

Figure 6. Isovelocity (dashed lines) and isothermal (solid lines) contours in a $z \times y$ plane at $x = 11$.

The streamwise evolution of Stanton number for Blasius and Goertler is shown in Fig. 7. It can be observed that until $x = 5$ the non-linear effects are small and the values os Stanton number with and without Goertler are the same. After this region, the non-linear effects increases, and the downwash region becomes more pronounced than the upwash region, increasing the Stanton number. The values at the streamwise position $x = 12.0$ are $St = 0.00065336$ and $St = 0.00171752$, with and without GV, respectively. This gives and increase of 162% in the number with the GV. This increase is lower than the increase in skin friction caused by the Goertler Vortices.

4.4 Analysis of heat transfer for $Pr = 7.07$

In the present section the results are for $Pr = 7.07$, therefore the hydrodynamic boundary layer is larger than the thermal boundary layer, as can be observed in Fig. 8, in the streamwise position $x = 11.0$. The downwash region is much larger than the upwash region and this is particularly observed for the thermal boundary.

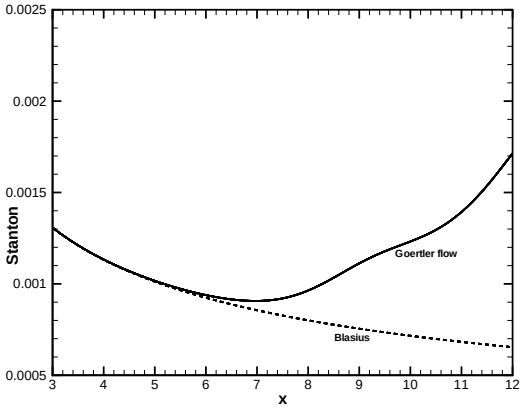

Figure 7. Streamwise evolution of the Stanton number. Dashed – Value obtained for the flow without GV. Thicker line – mean value with GV.

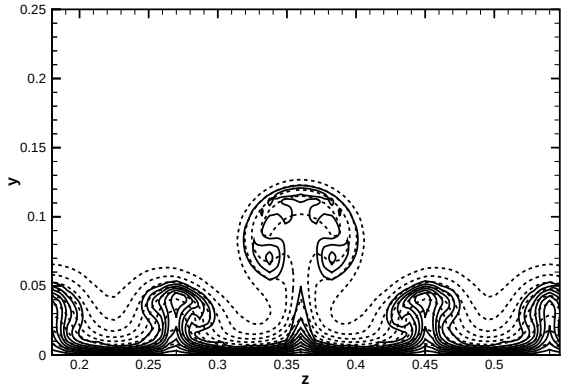

Figure 8. Isovelocity (dashed lines) and isothermal (solid lines) contours in a $z \times y$ plane at $x = 11$.

The same analysis of the Stanton number distribution in the streamwise direction was carried out, and the result is shown in Fig. 9. The values of Stanton number for Blasius and Goertler are respectively $St = 9.79687/times10^{-6}$ and $St = 4.1985343/times10^{-5}$. In the present case this represents an increase of 328% in this number. The increase in skin friction is 193%, as shown in section 4.1 Therefore, in the present case the gain in heat transfer is greater than the losses in skin friction. These results show that with the use of centrifugal instabilities in boundary layer, one can obtain higher heat transfer coefficient, when $Pr > 1$.

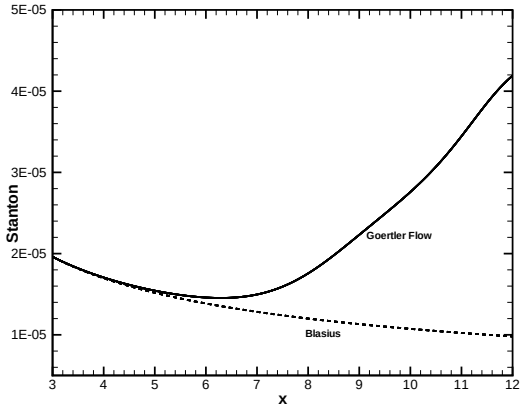

Figure 9. Streamwise evolution of the Stanton number. Dashed – Value obtained for the flow without GV. Thicker line – mean value with GV.

5. CONCLUSIONS

In the present work the heat rates over a concave surface are analyzed. The results shows that the heat transfer on a concave surface increases in the presence of Goertler vortices. An increase of 193% in the skin friction values was observed with the adopted configuration. The analysis of the heat transfer rates was done by Stanton number variation in the streamwise direction. It was observed that:

- For $Pr = 0.72$ the value of St increased 162% if compared to Blasius flow;
- For $Pr = 1.00$ the value of St increased 193% if compared to Blasius flow;
- For $Pr = 7.07$ the value of St increased 328% if compared to Blasius flow.

Therefore, these results show that the presence of Goertler Vortices in boundary layer, one can obtain higher heat transfer coefficient. For $Pr = 7.07$ the total gain in heat transfer rate is much greater than the skin friction. This behaviour should be same for $Pr > 1$, showing that this is a payoff system.

6. ACKNOWLEDGEMENTS

The authors acknowledge the financial support received from FAPESP under grant 2010/00495-1.

7. REFERENCES

Ferziger, L.F. and Peric, M., 1997. *Computational Methods for Fluid Dynamics*. Springer-Verlag Berlin Heidelberg, New York.

Fiebig, M., 1996. "Vortices and heat transfer". *Z. Angew. Math. Mech.*, Vol. 76, pp. 1–16.

Girgis, I.G. and Liu, J.T.C., 2006. "Nonlinear mechanics of wavy instability of steady nonliear longitudinal goertler vortices on a concave wall". *Phys. Fluids*, Vol. 18.

Kloker, M., Konzelmann, U. and Fasel, H.F., 1993. "Outflow boundary conditions for spatial navier-stokes simulations of transition boundary layers". *AIAA Journal*, Vol. **31**, pp. 620–628.

L. F. Souza, M.T.M. and Medeiros, M.A.F., 2005. "The advantages of using high-order finite differ- ences schemes in laminar-turbulent transition studies". *International Journal for Numerical Methods in Fluids*, Vol. 48, pp. 565–592.

L. Momayez, P.D. and Peershossaini, H., 2004. "Some unexpected effects of wabelenght and pertubation strength on heat transfer enhancement by goertler instability". *Int. J. Heat Mass Transfer*, Vol. 47, pp. 495–492.

Lele, S., 1992. "Compact finite difference schemes with spectral-like resolution". *J. Computational Physics*, Vol. 103, pp. 16–42.

Meitz, H.L., 1996. *Numerical Investigation of Suction in a Trasitional Flat-Plate Boundary Layer*. Ph.D. thesis, The University of Arizona.

Meitz, H.L. and Fasel, H.F., 2000. "A compact-difference scheme for the navier-stokes equations in vorticity-velocity formulation". *J. Computational Physics*, Vol. 157, pp. 371–403.

Souza, L.F., 2003. *Instabilidade centrífuga e transição para turbulência em escoamentos laminares sobre superfícies côncavas*. Ph.D. thesis, Instituto Tecnológico de Aeronáutica, Brazil.

Stüben, K. and Trottenberg, U., 1981. *Nonlinear multigrid methods, the full approximation scheme*, Köln-Porz, chapter 5, pp. 58–71.

Swearingen, J.D. and Blackwelder, R.F., 1987. "The growth and breakdown of streamwise vortices in the presence of a wall". *J. Fluid Mech.*, Vol. **182**, pp. 255–290.

8. Responsibility notice

The author(s) is (are) the only responsible for the printed material included in this paper